Numerical Analyses of MHD Flows in an Applied-Field MPD Arcjet Thruster

Hiroshi Katsurayama*, Takeshi Miyasaka† and Toshi Fujiwara‡
Department of Aerospace Engineering,
Nagoya University
Furo, Chikusa-ku, Nagoya, 464-8603, Japan

Abstract

Though heat loss is very large in an arcjet thruster of a several kW class, we think that the performance could be improved by inputting the part of a total input electric power in the form of the Lorentz work which is generated by an applied field. In order to analyze the behavior of swirl acceleration by this applied field in MHD flows, a numerical code of an axisymmetric model with the azimuthal momentum conservation is developed. This model takes into consideration viscosity, chemical nonequilibrium, and thermal nonequilibrium. The electric field is solved by FEM, and coupled with the flow field. Numerical results shows that the MHD flow is adequately accelerated to the azimuthal direction by the applied field and the input power is validly used in the form of Lorentz work. The effects on the thruster performance by the applied field are evaluated with the thrust, the thrust efficiency and the anode heat loss by the heat flux carried on discharge current. It is found out that the thruster performance is improved by the applied field. However, the improvement is not outstanding in spite of considerably intensive applied fields.

Nomenclature

$\mathbf{B}$	=	magnetic field vector
$\mathbf{E}$	=	electric field vector
e	=	total energy per unit volume, charge of electron
H_0	=	inflow enthalpy per unit mass
$\mathbf{i}, i$	=	mass diffusion flux
$\mathbf{j}, j$	=	current density
J	=	total current
k_B	=	Boltzmann constant
m	=	mass of particle
$\dot{m}$	=	mass flow rate
n	=	number density of particles
p	=	static pressure
$\mathbf{q}, q$	=	heat flux
T	=	temperature
T	=	thrust
V	=	discharge voltage
u, v, w	=	cylindrical components of velocity
z, r, θ	=	cylindrical coordinates
α	=	ionization degree
γ	=	specific heat ratio
δe_e	=	rate of electron energy exchange
ϵ_i	=	ionization potential
η, ξ	=	general coordinates
η	=	efficiency
κ	=	thermal conductivity
$\ln\Lambda$	=	Coulomb logarithm
μ	=	viscosity
ν	=	collision ferquency
ρ	=	mass density
$\dot{\rho}_i$	=	rate of ion mass production by reaction
σ	=	electric conductivity
τ	=	viscous stress
ϕ	=	electric potential
φ_i	=	ionization potential per unit mass

Subscripts

A	=	argon, ambipolar diffusion
e	=	electron
g	=	heavy species
i	=	ion
j	=	running index of species
L	=	Lorentz work
n	=	neutral
Q, q	=	anode heat loss
T	=	thrust

Introduction

The arcjet thruster is an electrothermal propulsion system, which heats gaseous propellant with Joule heat generated by an arc discharge from anode to cathode and then accelerates the propellant by an expansion in the nozzle. The arcjet has the advantages of simple structure and relatively higher thrust density compared with electrostatic propulsion systems. However, the arcjet has a serious problem in 1-10 kW operation conditions at the low voltage mode. Under this operating mode, the thrust efficiency is low because of the increased heat flux to the anode wall by the arc column attachment to the anode. One method for improvement is that the arcjet is operated at the high voltage mode in order to prevent the arc column attachment by stretching the current stream lines to the more downstream part of the thruster.

*Graduate student
†Research associate
‡Professor, Member AIAA

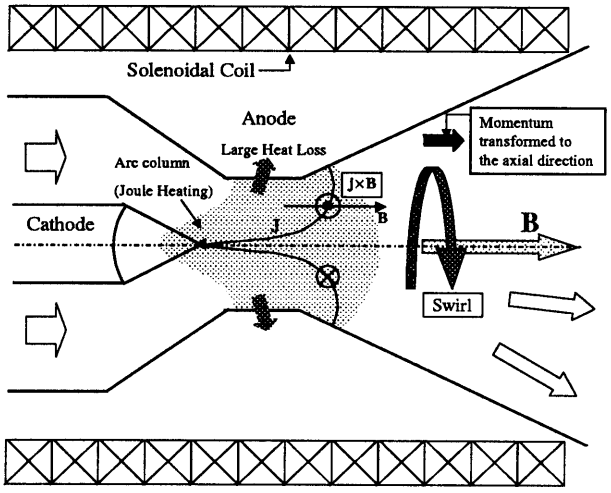

Fig. 1. The acceleration mechanism of an applied-field arcjet

This approach has been being studied by sophisticated numerical analyses and experiments[1]~[5]. Another method may be that part of the total input electric power is inputted in the form of an azimuthal kinetic energy.

The acceleration mechanism on this method is shown in Fig.1. An axial magnetic field is applied by a solenoidal coil, aligned coaxially with the thruster axis. An azimuthal Lorentz force is produced by the interaction between this applied field and the radial discharge current. This azimuthal force causes the swirl acceleration of the MHD flow. Consequently, the total input power is given to the plasma in the form of Lorentz work and Joule heat. Although some of the kinetic energy is converted into static enthalpy of the MHD flow, it can finally be converted into an axial kinetic energy through the solid nozzle. The hydrodynamic pressure exerted on the solid surface of the thruster contributes a thrust component[6]. Accordingly, the larger the ratio of power converted into the Lorentz work, the higher would be the thrust efficiency because of the less heat loss ratio on the total input power. Experiments, numerical and theoretical analyses on applied field MPD thrusters with several hundreds kW have been performed[6]~[9]. However, On 1-10 kW class arcjet thrusters, the effects of the applied field have never been investigated. In order to estimate the effects on the MHD flows by the applied field in 1-10 kW class arcjet thrusters, we performed numerical analyses with an axisymmetric 2-D model. This model incorporates the finite-rate ionization and recombination processes, and electron temperature disparity, to correctly capture the phenomena in the MHD flows.

Numerical model

Assumptions

As a first step for estimating the effects of swirl acceleration, the flow field and the electromagnetic field are simplified under the following assumptions.

1. The flow field is axisymmetric, and viscous. Physical properties have no gradient in azimuthal direction.
2. The gaseous propellant is argon which is considered a perfect gas, and plasma is quasi-neutral.
3. The electron temperature is in nonequilibrium with the translational temperature of heavy species.
4. The magnetic field is only an applied field. It is applied with a constant magnitude only to the axial direction along the thruster center axis. The self -induced field is negligible.
5. Only the following single-ionization and recombination process is considered. Therefore, electronic excitations are ignored.

$$\mathrm{Ar} + \mathrm{e} \rightleftharpoons \mathrm{Ar}^{+} + \mathrm{e} + \mathrm{e} \,. \qquad (1)$$

6. The effects of the magnetic field on transport phenomena and Hall current are ignored; the MHD flow is assumed isotropic.
7. The radiative energy transfers are ignored.

Governing equations

The equation system is described by the Navier-Stokes equations extended to chemical and thermal nonequilibrium gases. All fluid dynamics equations are expressed by an unsteady vector equation in conservation form.

$$\frac{\partial \mathbf{U}}{\partial t} + \frac{\partial \mathbf{F}}{\partial z} + \frac{\partial \mathbf{G}}{\partial r} = \mathbf{H} + \frac{\partial \mathbf{M}}{\partial z} + \frac{\partial \mathbf{N}}{\partial r} + \mathbf{S} \,. \qquad (2)$$

$$\mathbf{U} = \begin{bmatrix} \rho \\ \rho u \\ \rho v \\ \rho w \\ e \\ \rho_i \\ e_e \end{bmatrix}, \mathbf{F} = \begin{bmatrix} \rho u \\ \rho u^2 + p \\ \rho uv \\ \rho uw \\ (e+p)\,u \\ \rho_i u \\ e_e u \end{bmatrix}, \mathbf{G} = \begin{bmatrix} \rho v \\ \rho uv \\ \rho v^2 + p \\ \rho vw \\ (e+p)\,v \\ \rho_i v \\ e_e v \end{bmatrix},$$

$$\mathbf{H} = \frac{1}{r} \begin{bmatrix} -\rho v \\ -\rho uv + \tau_{zr} \\ -\rho v^2 + \rho w^2 + \tau_{rr} - \tau_{\theta\theta} \\ -2\left(\rho vw - \tau_{r\theta}\right) \\ -\left(e+p\right)v - q_r + u\tau_{zr} + v\tau_{rr} + w\tau_{\theta r} \\ -\rho_i v - i_{ir} \\ -e_e v - q_{er} \end{bmatrix},$$

$$\mathbf{M} = \begin{bmatrix} 0 \\ \tau_{zz} \\ \tau_{zr} \\ \tau_{z\theta} \\ u\tau_{zz} + v\tau_{zr} \\ \quad +w\tau_{z\theta} - q_z \\ -i_{iz} \\ -q_{ez} \end{bmatrix}, \quad \mathbf{N} = \begin{bmatrix} 0 \\ \tau_{zr} \\ \tau_{rr} \\ \tau_{r\theta} \\ u\tau_{zr} + v\tau_{rr} \\ \quad +w\tau_{r\theta} - q_r \\ -i_{ir} \\ -q_{er} \end{bmatrix},$$

$$\mathbf{S} = \begin{bmatrix} 0 \\ 0 \\ j_\theta B_z \\ -j_r B_z \\ \mathbf{j} \cdot \mathbf{E} \\ \dot{\rho}_i \\ \mathbf{j}^2/\sigma - \delta e_e \end{bmatrix} . \quad (3)$$

The total energy and electron energy per unit volume are defined as

$$e = \frac{p}{\gamma - 1} + \frac{\rho\left(u^2 + v^2 + w^2\right)}{2} + \varphi_i \rho_i \ . \quad (4)$$

$$e_e = \frac{p_e}{\gamma - 1} \ . \quad (5)$$

where the electron kinetic energy is neglected, $\gamma = 5/3$ and $\varphi_i = \epsilon_i / m_A$.
The static pressures are defined as

$$p = n_g k_B T_g + p_e \ . \quad (6)$$

$$p_e = n_e k_B T_e \ . \quad (7)$$

where $n_g = n_n + n_i$, and $n_e = n_i$ by the quasi-neutral assumption.
The viscous stress tensor is expressed as

$$\begin{bmatrix} \tau_{zz} & \tau_{zr} & \tau_{z\theta} \\ \tau_{rz} & \tau_{rr} & \tau_{r\theta} \\ \tau_{\theta z} & \tau_{\theta r} & \tau_{\theta\theta} \end{bmatrix} =$$

$$\mu \begin{bmatrix} 2\frac{\partial u}{\partial z} - \frac{2}{3}\nabla \cdot \mathbf{u} & \frac{\partial v}{\partial z} + \frac{\partial u}{\partial r} & \frac{\partial w}{\partial z} \\ & 2\frac{\partial v}{\partial r} - \frac{2}{3}\nabla \cdot \mathbf{u} & \frac{\partial w}{\partial r} - \frac{w}{r} \\ sym. & & 2\frac{v}{r} - \frac{2}{3}\nabla \cdot \mathbf{u} \end{bmatrix} . \quad (8)$$

where

$$\nabla \cdot u = \frac{\partial u}{\partial z} + \frac{\partial v}{\partial r} + \frac{v}{r} \ . \quad (9)$$

The ion mass diffusion vector and heat flux vector of heavy species are defined as

$$\mathbf{i}_i = -D_A \nabla \rho_i \ . \quad (10)$$

$$\mathbf{q}_g = \varphi_i \mathbf{i}_i - \kappa_g \nabla T_g \ . \quad (11)$$

Taking account of the deflection of mass center velocities between electron and heavy species, the heat flux vector is defined in the following form[1],

$$\mathbf{q}_e = -\kappa_e \nabla T_e - \frac{\gamma k_B T_e}{(\gamma - 1)\, e}\mathbf{j} \ . \quad (12)$$

Total heat flux vector is expressed by adding the heat flux vectors of heavy species and electron.

$$\mathbf{q} = \mathbf{q}_g + \mathbf{q}_e \ . \quad (13)$$

Electron translational energies are transfered by collisions against heavy species. The rate of its energy transfer is defined as

$$\delta e_e = \left(\nu_{en} + \nu_{ei}\right) n_e k_B \left(T_e - T_g\right) + \varphi_i \dot{\rho}_i \ . \quad (14)$$

where the first term is the energy transfer in the elastic collisions, and the second term in the inelastic collisions with ionizations and recombinations.

Electromagnetic field

In an applied field arcjet, Hall current may be large especially in the nozzle, where the MHD flow has low density. However, In the present study, Hall current is ignored for simplicity, as the first step to estimate the swirl acceleration. The magnetic field is assumed as the only applied field which has the only a component of the axial direction. In addition, by ignoring the term with respect to the gradient of electron pressure, the generalized Ohm's law is written as the following,

$$\mathbf{j} = \sigma\left(\mathbf{E} + \mathbf{u} \times \mathbf{B}\right) \ . \quad (15)$$

The components of current density are expressed as the following,

$$j_r = \sigma\left(E_r + wB_z\right) \quad (16)$$

$$j_\theta = -\sigma v B_z \quad (17)$$

$$j_z = \sigma E_z \quad (18)$$

From Eq.(15) and steady-state Maxwell equations, the following elliptic equation is derived with respect to the electric potential ϕ on the axisymmetric coordinate.

$$\frac{\partial}{\partial z}\left(r\sigma\frac{\partial \phi}{\partial z}\right) + \frac{\partial}{\partial r}\left(r\sigma\frac{\partial \phi}{\partial r}\right) = \frac{\partial}{\partial r}\left(rwB_z\right) \ . \quad (19)$$

Transport properties

Transport phenomena occur by virtue of random collisions among particles within the plasma. Therefore, different transport phenomena occur by virtue of collisions among different kinds of particles. In slightly ionized plasmas, there are relatively few charged particles and thus the motions of the neutrals play the dominant role in transport phenomena. However, if the level of ionization is relatively high, the collisions among the charged particles must also be considered as well as collisions among neutrals and charged particles. Because the arcjet has both the slightly ionized domains and highly ionized domains, transport properties need be estimated taking into consideration these two different collision processes. For example, for the electric conductivity,

$$\sigma_L = \frac{n_e e^2}{m_e \sum_j \nu_{ej}} \ . \quad (20)$$

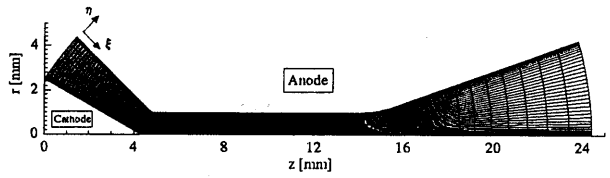

Fig.2. Thruster geometry and grids (165 × 40)

$$\sigma_H = 1.53 \times 10^{-2} \frac{T_e^{3/2}}{\ln\Lambda} \ [\mathrm{S}] \ . \qquad (21)$$

The former is for the slightly ionized plasma based on Chapman-Cowling theory, the latter is for the highly ionized plasma introduced by L.Spitzer. In the present study, the substantial electric conductivity is defined as the following[10],

$$\sigma = \frac{\sigma_L \sigma_H}{\sigma_L + \sigma_H} \ . \qquad (22)$$

Though other properties with respect to charged particles are similarly defined, the viscosity of the whole fluid is defined by adding viscosities of ions and neutrals. Additionally, as for the diffusion of ions, the following ambipolar diffusion coefficient is adopted,

$$D_A = (1 + T_e/T_g)\, D_i \ . \qquad (23)$$

All transport properties perpendicular to a magnetic field are smaller than properties parallel to the field, because of charged particles being captured by the field. However, the present model ignores this effect for simplicity.

Numerical Procedure

Fig.2 shows the schematic picture of the grid system. It is the same shape as The Nagoya Univ. Arcjet Thruster Second (NUATII). The constrictor of NUATII is considerably long so as to effectively use the applied field of the solenoidal coil.

In order to save calculation costs, the upstream end of the calculation domain is extended to the end of the cathode cone, and the downstream end is limited to one third of the nozzle length of NUATII, where the flow is adequately supersonic. In the general coordinate system (ξ, η), the grid points are 165 × 40, where the cells are clustered near the both electrode surfaces, the upstream edge of constrictor and the cathode tip in order to resolve the steep gradients of physical properties. The constrictor radius is 1.0mm, The constrictor length is 10.0mm, and the axial gap between the cathode tip and the constrictor upstream edge is 0.5mm.

The fluid dynamic equation vector transformed to this general coordinate is solved using the Harten-Yee's 2nd-order- accurate fully explicit symmetric TVD scheme[11], where the time increment is determined by the CFL condition.

On the other hand, the electric field is determined at every time-step of the flow field, by solving the Eq. (19) using the FEM under the assumption that the electric field is steady-state for the flow field.

Boundary conditions

At the inlet boundary, the flow is assumed subsonic. Therefore, one of the independent variables should be determined from downstream. In the present study the static pressure is determined form downstream by the zeroth order extrapolation for simplicity. The mass flow rate is specified as the operating parameter, the total enthalpy is specified to 300K, the azimuthal velocity is set to zero in order to purely estimate the swirl acceleration by the applied field. The number densities of the charged particles are set to zero, and the electron temperature is set equal to the heavy species temperature. Then, the velocity, density, and temperature are obtained by the energy conservation law using the above mentioned values.

At the exit boundary, the flow is assumed supersonic by neglecting the influence of the subsonic region near the anode wall. Therefore, Physical properties are determined from upstream by the zeroth order extrapolation.

On the electrode boundaries, the viscous nonslip condition is imposed. The normal gradient of the static pressure is set to zero. The normal gradients of both the electron temperature and the number density of charged particles, are also set to zero. In other words, the electrode walls are assumed as non-catalytic. Therefore, detailed physical aspects near the electrodes are ignored. The cathode wall temperature increases linearly from 300K at the inlet, to 3600K at the cathode tip. The anode wall temperature increases linearly from 300K at the inlet, to 1600K at the upstream edge of the constrictor. The constrictor wall temperature is constant value, 1600K. And the anode wall temperature decreases linearly form this value to 500K at the end of the nozzle. The temperatures of both electrodes are fixed. The temperatures of the heavy species are set equal to both electrode temperatures.

On the center axis, the axisymmetric condition, in which the azimuthal and radial component of the velocity are set to zero, is imposed. The normal gradients of other physical properties are set to zero.

As for the boundary conditions on the electric field, the discharge voltage is imposed as the cathode surface negative potential with respect to the anode. This potential of the cathode is controlled for the calculated total discharge current to become equal to the value of the operating parameter. On the inlet, center axis, and exit boundary, the natural boundary condition is satisfied.

Results and Discussion

Calculations are conducted in the cases of applied fields of B = 0.00T, 0.25T and 0.50T with the total discharge current of J = 80A and the mass flow rate of $\dot{m}$ = 0.1g/s.

The case without an applied field

The current stream lines in the case of B = 0.00T are shown in Fig.3. The arc current stream lines attach to the anode surface of the region from the middle of the cathode to the vicinity of the constrictor upstream edge, and the discharge is mainly conducted in this region. we hereafter refer this region as the discharge region. This result shows that the thruster is operated in the low voltage mode, in accordance with many experiments and calculations using argon as the propellant.

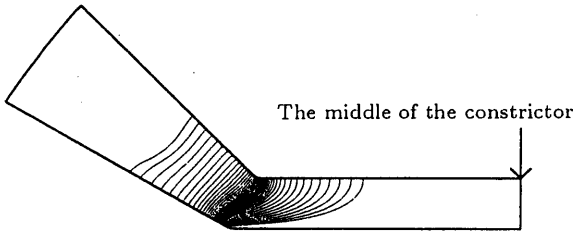

Fig.3. Current stream lines in the discharge region without an applied field.

The cases with applied fields

The contour of the azimuthal velocity for B = 0.50T is shown in Fig.4. The maximum velocities are w = 912.4m/s and 1168.6m/s in the cases of B = 0.25T and 0.50T, respectively. The axial profiles of the azimuthal Lorentz force, $j_r B_z$, and the azimuhtal velocity in the region, which is from the inlet to the middle of the constrictor, are shown in Fig.5 and Fig.6. The arc discharge is almost finished beyond the constrictor upstream edge as same as the case of B = 0.00T. Therefore, the azimuthal acceleration by Lorentz force is also finished beyond the constrictor upstream edge. In the constrictor region, the azimuthal velocity gradually decreases by the viscosity with the constrictor wall. However, the rate of the decrease becomes slower with approaching the constrictor wall because the azimuthal momentum is transfered to radial direction by viscous momentum transfer from the vicinity of the center line where the azimuthal velocity has the largest value.

In order to estimate how the input power is used as Lorentz work per unit volume, we introduce the following ratio,

$$\eta_L \equiv \frac{\text{Lorentz work per unit volume}}{\text{Supplied power per unit volume}} = \frac{|w j_r B_z|}{\mathbf{j}\cdot\mathbf{E}} . \tag{24}$$

Figure.7 shows the radial profiles of η_L from the cathode tip to the constrictor upstream edge. The larger magnetic fields are applied, the larger becomes η_L. In these cases of B = 0.25T and 0.50T, the maximums of η_L are about 2% and 7%, respectively. Thus, it is concluded that input power is validly transformed to Lorentz work.

Fig.4. Azimuthal velocity contour for B = 0.50T. (max.=1168.6m/s, min.=0.0m/s, increment= 100.0m/s)

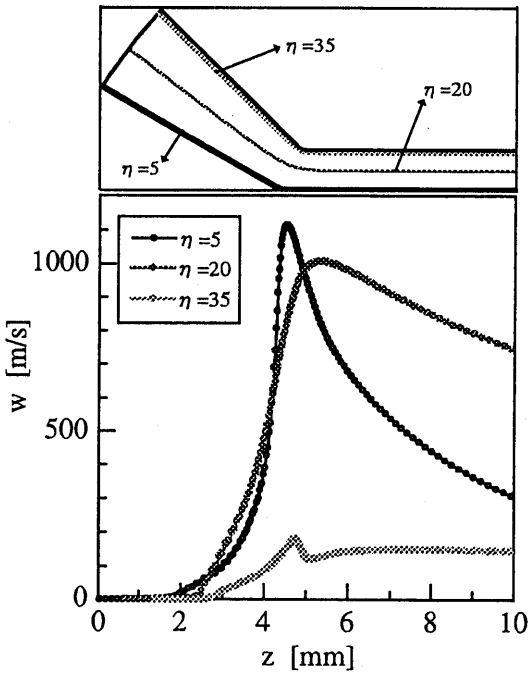

Fig.5. Azimuthal velocity profiles from the inlet to the middle of the constrictor for B = 0.50T.

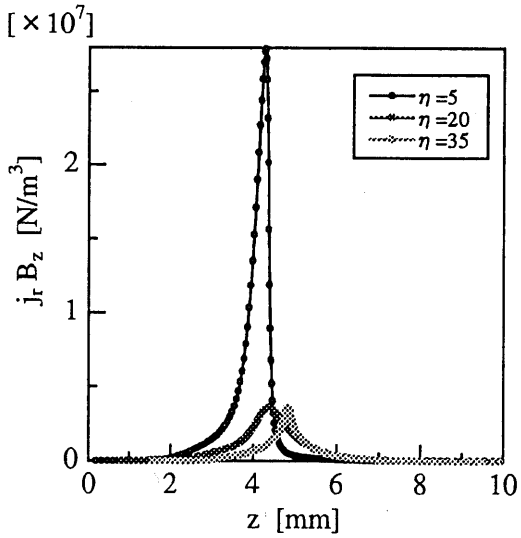

Fig.6. Lorentz force profiles from the inlet to the middle of the constrictor for B = 0.50T.

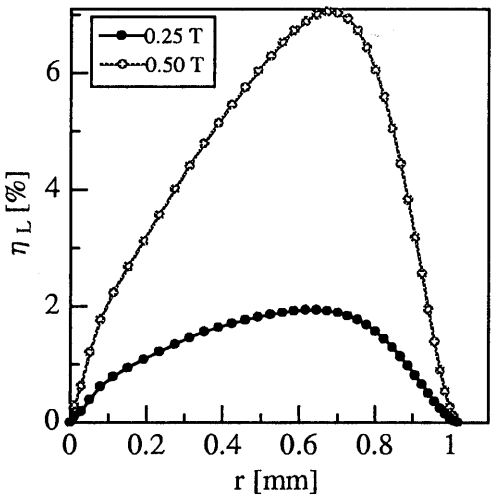

Fig.7. Radial profiles of η_L from the cathode tip to the constrictor upstream edge.

Performance estimations with applied fields

In order to estimate the effect on the thruster performance by applied fields, the following ratios are defined.

The Lorentz efficiency is defined as

$$\eta_{L\,overall} \equiv \frac{\text{Overall Lorentz work in thruster}}{\text{Inflow enthalpy and total input power}} = \frac{\int |w j_r B_z|\, dv}{VJ} . \quad (25)$$

The thrust efficiency is defined as

$$\eta_T \equiv \frac{\text{Axial thrust energy}}{\text{Inflow enthalpy and total input power}} = \frac{T^2}{2\dot{m}\,(VJ + \dot{m}H_0)} . \quad (26)$$

With respect to the estimation of the heat loss to the anode, the most important factor is the heat flux carried on discharge current. Accordingly, the heat flux carried on discharge current is only considered as the following,

$$\eta_Q \equiv \frac{\text{Total heat flux to andoe by current}}{\text{Inflow enthalpy and total input power}} = \frac{\int_{\text{anode wall}} \frac{\gamma k_B T_e}{(\gamma-1)\,e}\,(j_r^2 + j_z^2)\, dS}{(VJ + \dot{m}H_0)} . \quad (27)$$

$\eta_{L\,overall}$ is shown in Fig.8. And η_T, η_Q and thrust are shown in Fig.9. $\eta_{L\,overall}$ for $B = 0.50$T is about three times as large as the $\eta_{L\,overall}$ for $B = 0.25$T. Thus, these estimations of $\eta_{L\,overall}$ also prove the validity of the applied field.

The thrust and η_T also increase with applied fields in Fig.9. Figure.10 shows the profiles of the integral values over the η direction's cross-sections of the azimuthal kinetic energies in the region where is from the vicinity of the constrictor downstream end to the nozzle end. Though the azimuthal kinetic energy with $B = 0.50$T is larger than one with $B = 0.25$T at the constrictor downstream end, the azimuthal kinetic energies of the both cases become almost same values at the nozzle end. This fact implies that the azimuthal kinetic energies are adequately transformed to the axial kinetic energies by the solid nozzle.

The heat loss to the anode caused by the heat flux carried on discharge current decreases with applied fields. For the purpose of estimation of the dependence of the heat flux distributions along the anode on applied fields, the following non-dimensional value is introduced. The values of η_q in the discharge region and the enlarged figure near the constrictor upstream edge are shown in Fig.11.

$$\eta_q = \frac{\left[2\pi r_a \frac{\gamma k_B T_e}{(\gamma-1)e}\,(j_r^2 + j_z^2)\right] R_c}{VJ} . \quad (28)$$

where r_a is the radius of the anode and R_c is the constrictor radius which is multiplied as the representative length used for non-dimensionalization. The value of η_q for each applied field has the peak at the constrictor upstream edge. The peak value of η_q becomes lower for a stronger applied field. This is because the counter-electromotive force, wB_z, in Eq.(16), increases with the applied field near the constrictor upstream edge.

Consequently, these results of efficiencies indicate the improvement of thrust performance by applying the magnetic field. However the improvement is not outstanding in spite of considerably intensive applied fields. The one of the causes is the decrease of the azimuthal velocity in the constrictor due to the existence of viscosity. As the arc discharge is conducted near the constrictor upstream edge in the low voltage mode, the long constrictor used in the present study, which intend to use an applied field validly, does not need. Therefore, the shorter constrictor seems to improve the performance more strongly.

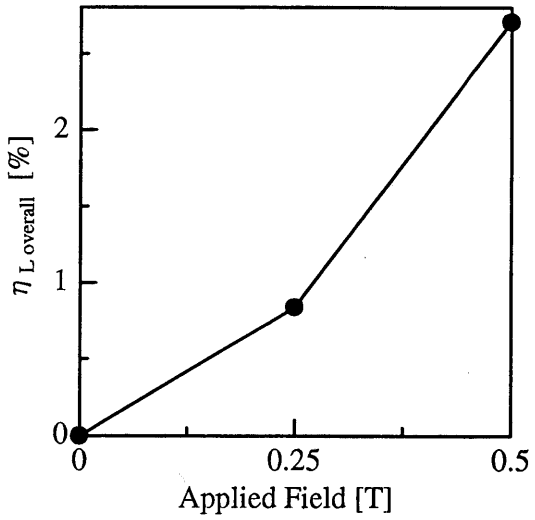

Fig.8. The Lorentz efficiency on the whole of the thruster.

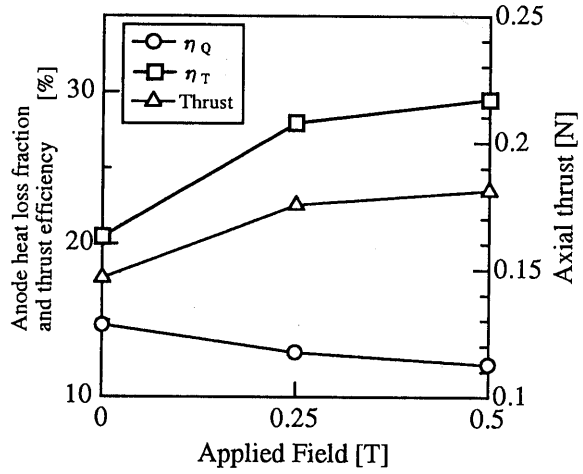

Fig.9. Anode heat loss fraction, thrust efficiency and thrust.

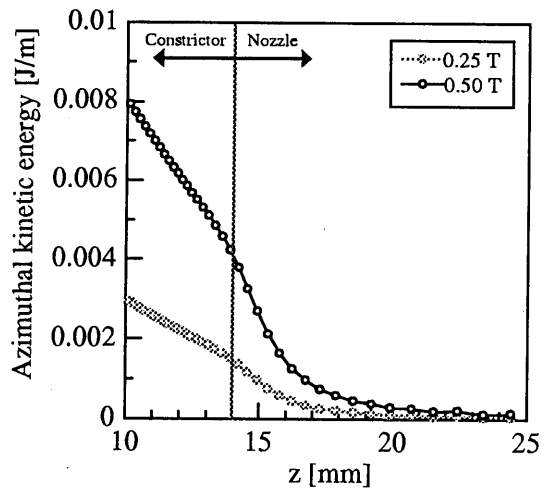

Fig.10. The profiles of the integral values over the η direction's cross-sections of the azimuthal kinetic energies from the vicinity of the constrictor downstream end to the nozzle end.

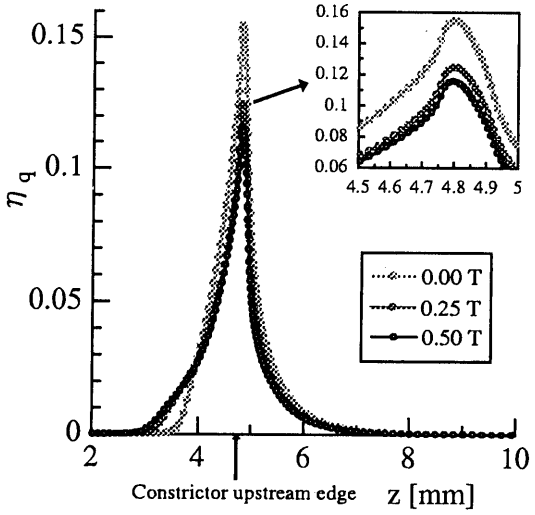

Fig.11. The profiles of η_q in the discharge region and the enlarged figure near the constrictor upstream edge

Conclusion

Numerical results shows that the MHD flow is adequately accelerated to the azimuthal direction by the applied field and the input power is validly used in the form of Lorentz work.

The effects on the thruster performance by the applied field are evaluated with the thrust, the thrust efficiency and the anode heat loss by the heat flux carried on discharge current. It is found out that the thruster performance is improved by the applied field. However, the improvement is not outstanding in spite of considerably intensive applied fields. To improve the performance strongly by the applied field, the thruster with the short constrictor seems to be more valid.

Moreover speaking, the applied field would become more valid on the high voltage mode than the low voltage mode because the azimuthal acceleration would be conducted in the nozzle and the azimuhtal momentum would be quickly transformed to the axial momentum by the current stream lines stretched to the nozzle.

We will focus future efforts on the applied field arcjet with the high voltage mode and the short constrictor.

References

[1] Fujita, K., "Performance Computation of a Low-Power Hydrogen Arcjet," AIAA Paper 96-3183, July 1996.

[2] Fujita, K., and Arakawa, Y., "Numerical Prediction of Arcjet Performance Based on the Chemical Kinetics and Electron Temperature Disparity," *Proceedings of the 24th International Electric Conference*, Moscow, 1995, pp.183-192.

[3] Kuchi-ishi, S., and Nishida, M., "Numerical Simulation of a Nitrogen Arcjet Thruster," Transactions of the Japan Society for Aeronautical and Space Sciences, Vol.42, No.136, 1999, pp.69-75.

[4] Auweter-Kurtz, M., Gölz, T., Habiger, H., Hammer, F., Kurtz, H., Riehle, M., and Sleziona, C., "High-Power Hydrogen Arcjet Thrusters," Journal of Propulsion and Power, Vol.14, No.5, Septr-Oct, 1998.

[5] Miller, S. A., Martinez-Sanchez, M., "Two-Fluid Nonequilibrium Simulation of Hydrogen Arcjet Thrusters," Journal of Propulsion and Power, Vol.12, No.1, Jan-Feb, 1996.

[6] Sasoh, A., and Arakawa, Y., "Thrust Formula for an Applied MPD Thruster Derived from Energy Conservation Equation," *Proceedings of the 22nd International Electric Conference*, Viareggio, Italy, 91-062, 1991.

[7] Thomas, H., Chapman, R., and Garrison, G. W., "A Numerical Simulation of Axisymmetric, Steady-State Plasma Flow Through MPD-Type Thrusters With Applied Magnetic Fields," AIAA Paper, 1992

[8] Tanaka, M., and Kimura, I., "Current Distribution and Plasma Acceleration in MPD Arcjets with Applied Magnetic Fields," Jornal of Propulsion and Power, Vol.4, No.5, Sept-Oct. 1988. pp.428-436.
[9] Myers, R.M., "Scaling of 100 kw Class Applied-Field MPD Thrusters," AIAA Paper 91-3462, July 1992.
[10] Cambel, A.B., "Plasma Physics and Magnetofluidmechnics," McGraw-Hill Book Company. New York, pp152-195, Chap.7, 1963.
[11] Yee, H.C., "A Class of High-Resolution Explicit and Implicit Shock-Capturing Methods," NASA-TM 101088, 1989.